archives
of thermodynamics
Vol. **41**(2020), No. 4, 93–114
DOI: 10.24425/ather.2020.135855

Numerical research of combustion with a minimum boiler load

BARTŁOMIEJ HERNIK[a*]
WIESŁAW ZABŁOCKI[b]

[a] Department of Power Engineering and Turbomachinery, Silesian University of Technology, Konarskiego 18, 44-100 Gliwice, Poland

[b] RAFAKO S.A., Łąkowa 33, 47-400 Racibórz, Poland

Abstract Power boilers should be characterized by high flexibility in terms of loads, which results from the demand for electricity. In addition to the flexibility of the boiler, it is also important for the boiler to operate under technical minimum conditions while maintaining harmful emissions standards. A boiler operating with a technical minimum should also exhibit a stable combustion process. The paper presents the results of numerical combustion research for the minimum load of the two-pass ultra-supercritical boiler with front wall swirl burners system. The combustion stability for the minimum boiler load of 40% for the three mill system configurations has been demonstrated. Based on the numerical tests carried out in terms of obtaining the most favourable combustion conditions and the emission of harmful substances, the most favourable of them cases was indicated.

Keywords: Numerical simulations; Ultra-supercritical boiler; Coal combustion; Minimum boiler load

1 Introduction

Power plants, despite the increasingly propagated and advanced technology of using renewable sources or distributed energy, will remain for the next

*Corresponding Author. Email: bartlomiej.hernik@polsl.pl

several years, a major energy producer. The development of modern technologies for the use of renewable and zero-emission energy sources is very important. However, until the energy based on fossil fuels is eliminated, it is important to improve and develop low-carbon combustion technologies to meet the requirements of harmful emissions standards [1, 2].

Numerical modelling can and should be used to study the combustion process in the furnace chamber. Numerical tests are often associated with lower financial outlays and provide greater possibility of variants in the design and construction process as compared to laboratory or industrial tests. Nevertheless, it is very important to create numerical models based on measurements or zero-dimensional calculation models to authenticate numerically obtained results.

Currently, numerical modelling of the combustion process for models including the combustion chamber together with the second boiler pass is quite commonly used [3–5]. As a rule, numerical calculations are carried out to modernize or optimize the combustion process in boilers [6–11] or tests on a real object [12]. On the other hand, with a few exceptions [13–15], not much research was carried out on boiler combustion for minimal boiler load.

In [10] numerical calculations of a coal-fired boiler for variable load and fuel granulation were carried out to reduce SO_2/NO_x emissions. Chen *et al.* [12] presented a model of anthracite combustion and NO_x formation for a 300 MWe boiler fired with swirl burners for 3 loads after implementing a new combustion system. The distribution of secondary air from the burners to the nozzles of the OFA (Over fire air) nozzle group results in increased reheated steam temperature for lower loads, reduced NO_x emissions and improved combustion quality. In [13] the results of numerical modelling of a lignite fired boiler are presented for three loads, including one below the technical minimum. To obtain a load below the technical minimum of the boiler, co-firing with pre-dried fuel was used. The reduction of the minimum load and NO_x emissions in a lignite fired boiler was achieved by applying the stable flame concept [14]. A new concept for lignite combustion has been presented, leading to improved combustion stability and reduced NO_x emissions. Tan *et al.* [15] presented the results of research on the causes of flue gas temperature deviations in tower tangentially fired boilers. One method to solve the problem is to add an arched nose before the boiler draft.

Power boilers should work with high flexibility in terms of loads, which results from the demand for electricity. In addition to the flexibility of the boiler, it is also important for the boiler to operate under technical mini-

mum conditions while maintaining harmful emissions standards. A boiler operating with a technical minimum should also exhibit a stable combustion process. The article presents the results of numerical combustion research for the minimum load of the two-pass ultra-supercritical boiler with front wall swirl burners system – BP 680 boiler, specified in the design phase at Rafako factory. Computational fluid dynamics (CFD) modelling for a 100% boiler load is presented in [16, 17].

2 Boundary conditions and modelling description

The BP 680 boiler is a two-pass boiler for ultra-supercritical parameters, fired with hard coal dust, with steam reheated. The profile of the BP 680 boiler is shown in Fig. 1. The combustion chamber has a cuboid shape with transverse dimensions of 15.62 m × 9.02 m. Located just above the combustion chamber is the platen superheater (SH2b) The last fourth stage of the live steam superheater (SH4) is above SH2b. Over its the second stage

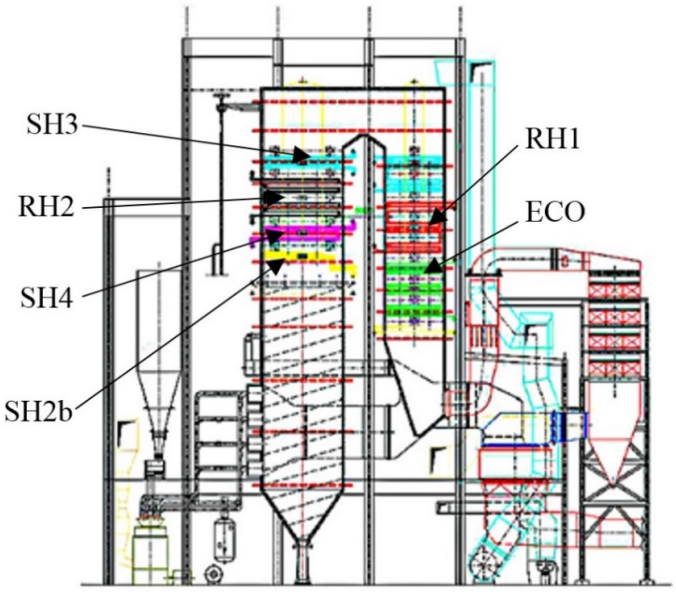

Figure 1: Cross-section in the axis of the BP 680 boiler, SH2b – platen superheater, SH4 – the last fourth stage of the live steam superheater, RH2 – the second stage of reheated steam, SH3 – the third stage of live steam superheater, RH1 – the first stage of the reheated steam, ECO – economizer.

of reheated steam (RH2) is localized. Around the draft the third stage of live steam superheater (SH3) is presented. Then on the flue gas path the first stage of the reheated steam (RH1) is showed. The economizer (ECO) is the last surface in the second pass.

BP 680 is fed by four mills (M1–M4), each supplying a pulverized coal-air mixture to six swirl burners located on the front wall of the furnace – Fig. 2. The burners are fed from a common secondary air box. Above the belt of burners on the front wall of the combustion chamber there are 6 OFA nozzles built-in, equipped with blades swirling the air at an angle of 45°.

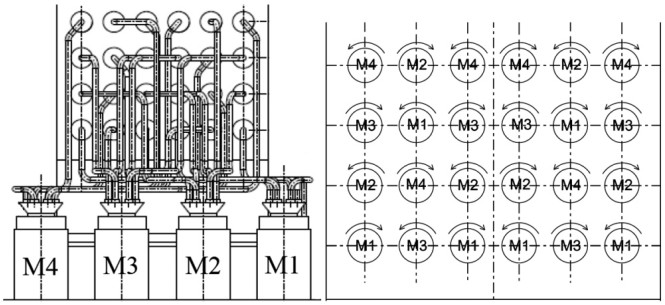

Figure 2: Mills system with marked burners swirl direction.

Figure 3 shows the burner diagram. The burner is divided into two sections of secondary air equipped with blades swirling the air at an angle of 50°.

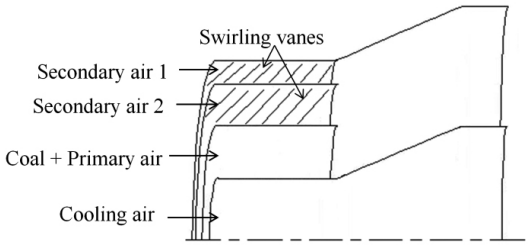

Figure 3: The diagram of the burner.

Table 1 presents the coal analysis provided by Rafako, which are the basis for developing input data for CFD software. Table 2 shows fuel granulation with average diameter of the coal dust particle used in the discrete phase model (DPM).

Table 1: Coal analysis.

Data	Unit	Value
Calorific value	kJ/kg	21500
Ash content	% by mass	22.00
Moisture content	% by mass	11.30
Volatile matter content	% by mass	37.60
Coal, C	% by mass	56.80
Hydrogen, H	% by mass	2.66
Sulphur, S	% by mass	1.24
Oxygen, O	% by mass	4.80
Nitrogen, N	% by mass	1.20

Table 2: Fuel grain size.

Data	Unit	Value
Residue on 90 µm sieve	%	15.00
Residue on 200 µm sieve	%	0.48
Average diameter	m	53×10^{-6}
Polydispersity number	–	1.26

For a 40% load, tests were carried out for the three mill system configurations:

1. Case 1 – chamber is powered by mills M1, M3; lower flame position.
2. Case 2 – chamber is powered by mills M1, M4; average flame position.
3. Case 3 – chamber is powered by mills M2, M4; upper flame position.

Table 3 demonstrates the air and fuel streams implemented into the numerical model and their temperatures. The data is the result of boiler balance calculations and was provided by Rafako.

The contour of the combustion chamber of the BP 680 boiler, the geometric model and the numerical mesh, which is built of 3 768 850 numerical cells, are showed in Fig. 4. The maximum value for skewness is 0.96 for 400 cells located in the flow part of burners and OFA nozzles not involved in the combustion process. The skewness factor in the range from 0 to 0.1 represents 87% of all grid cells, whereas the skewness factor in the range from 0.8 to 0.9 accounts for 13% of the mesh and occurs in the flow part of the OFA burners and nozzles. A minimum cell volume of 1.59^{-6} m^3 occurs in the area of the burner belt. However, the maximum cell volume

Table 3: Air and fuel flows.

Data	Unit	Mills								
		Case 1			Case 2			Case 3		
		1	3	2, 4	1	4	2, 3	2	4	1, 3
Coal mass flow	kg/s	5.65	5.65	–	5.68	5.68	–	5.72	5.72	–
Primary air mass flow	kg/s	14.32	14.32	–	14.41	14.41	–	14.51	14.51	–
Secondary air mass flow 1	kg/s	14.71	14.71	7.06	14.89	14.89	7.06	15.09	15.09	7.05
Secondary air mass flow 2	kg/s	10.11	10.11	4.85	10.24	10.24	4.85	10.37	10.37	4.85
Cooling air mass flow (core)	kg/s	1.65	1.65	1.65	1.65	1.65	1.65	1.65	1.65	1.65
Air mass flow to OFA	kg/s	20.11								
Mixture temperature	°C	100								
Secondary air temperature	°C	309			310			308		

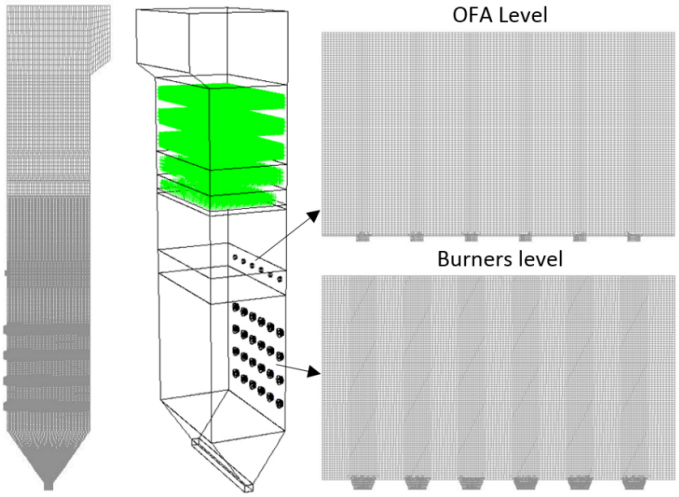

Figure 4: Geometrical model and numerical mesh in the cross-section of the BP 680 boiler.

of 2.13^{-2} m^3 occurs in the area of steam superheaters. The mesh in the region of the burners has been compacted in order to obtain more credible results. The model contains the first pass of the boiler, including steam superheaters. The superheaters were treated as a porous body made in the shape of plates, exchanging heat with flue gas. The standard energy transport equation with modifications of the conduction flux were solved in the porous body. In the porous medium, standard turbulence equations were

solved as in the mass flow of fluid. The turbulence is regarded as if the solid medium did not affect the rate of dissipation and the generation of turbulence. Inside the porous body the superficial velocity was used based on the volumetric flow rate. The porous body was modelled by defining an additional momentum source in the momentum equations for superheater areas:

$$S_i = -\left(\frac{\mu}{\alpha}\nu_i + C_2\frac{1}{2}\rho\,|\nu|\,\nu_i\right),$$

where S_i is the momentum equation for i-th (x, y, z) directions; $|\nu|$ is the magnitude of the velocity; ν is dynamic viscosity; $1/\alpha = D$ means viscous loss term based on Darcy's Law; C_2 means inertial loss term. Knowledge of the heat exchanger geometry allows calculating in the zero-dimensional model pressure drop, Δp, and flue gas velocity, v. Pressure drop as a function of velocity through a porous zone can be extrapolated to specify the D and C_2 coefficients. The following equation should be used to calculate the pressure drop:

$$\Delta p = \zeta\frac{\rho_{fg}\nu_{fg}^2}{2},$$

where ζ is the number of resistance, ρ_{fg} is the density of the flue gas, ν_{fg} is the velocity of the flue gas. In Table 4 values of porosity, viscous resistance as well as internal resistance for porous zone was presented.

Table 4: Characteristic parameters of the porous zone.

Data	Porosity	Viscous resistance	Internal resistance
Unit / Zone	–	$1/m^2$	1/m
SH2b	0.55	1.60×10^5	21.45
SH4	0.61	2.09×10^6	239.72
RH2	0.66	2.33×10^7	2266.5
SH3	0.67	1.48×10^7	1234.02

Based on calculations with the zero-dimensional model, the amount of heat received from the flue gas by steam was determined. Thus, this amount of heat flux is included in the calculations as a negative heat source for individual superheaters.

Numerical tests of the combustion process in the BP 680 boiler were carried out using the Ansys Fluent 14 simulation software [18]. The CFD

model has been verified by design calculations performed using the zero-dimensional Rafako model. Thanks to it, the flue gas temperature in the plane of the combustion chamber outlet was obtained. The oxygen content was obtained by performing stoichiometric calculations based on the coal composition. The model performs heat-flow balance calculations of the entire boiler, taking into account all heat exchange surfaces in the direction of flow and their characteristic dimensions. The heat transfer between flue gas and the working fluid, including fouling and heat preservation of tubes coefficients, is taken into account. The model provides the temperature of the flue gas and working fluid behind each heat exchanger as well as information about its velocity. The water-walls of the furnace chamber were modelled as flat surfaces exchanging heat with the flue gas.

Calculations were carried out in a steady state. At the beginning of calculations, the first order upwind scheme was used for momentum, turbulence, species, energy, and radiation. For a more accurate solution, when the model has stabilized, a second order upwind scheme was used for them. For pressure spatial discretization PRESTO (pressure staggering option) scheme was used. Least squares cell based scheme was used to simulate gradient spatial discretization. The walls were modeled as flat surfaces exchanging heat with the flue gas. For walls in the combustion chamber the temperature of 377 °C and an internal emissivity of 0.57 were set. The wall thickness corresponding to the wall thickness of the pipe in furnace was set to 0.004 m. For walls of the slag hopper the temperature of 296 °C and an internal emissivity of 0.5 were set. The research used the SIMPLE method (semi-implicit method for pressure linked equations) to valuation the flow fields [10, 19–22, 29]. The k-ε real turbulence model was also used due to calculations of boilers equipped with swirl burners. The choice of this model is a compromise between accuracy and calculation time, although it is no less appropriate to simulate a vortex turbulent flow [3, 4, 20, 21, 23, 24, 27, 29]. The Euler–Lagrange approach is more precise than the Euler–Euler approach in coal combustion calculations [3, 4, 19–21, 24, 25, 27, 29]. The Lagrange approach was used to calculate the trajectory of a coal particle in a continuous phase. 3960 particles have been tracked. The heat, mass and momentum exchange between coal particles and flue gas was simulated using the discrete phase model. The ability to model coal degassing and char burning is the highest advantage of the Euler–Lagrange two-phase approach. Coal degassing was modelled using the single rate model [21, 25, 26]. In turn, the combustion of char particles was modelled using a kinetic diffusion model [5, 6, 8, 19–21, 25, 27]. The char oxidation reaction to CO_2

according to this model is shown below:

$$C + O_2 \rightarrow CO_2 \,.$$

Fuel and thermal nitrogen oxides were included in the calculations [6, 7, 19] and turbulent interaction as a function of probability density (PDF) was determined.

For the calculation of the formation of thermal nitrogen oxides the Zeldowicz mechanism was used [30]. By providing energy in the oxygen particle, chains are intermittent and free O atoms can take part in the reaction:

$$O + N_2 \leftrightarrow NO + N,$$

$$N + O_2 \leftrightarrow NO + O.$$

Under circumstances congruous to stoichiometric and for mixtures rich in fuel, a third reaction was suggested, which contributes to the formation of thermal nitrogen oxides [31–33]

$$N + OH \leftrightarrow NO + H.$$

The concentration of O radicals was determined by applying the partial equilibrium approach [34]. To determine the concentration of OH radicals, an approach based on partial equilibrium was used [35, 36]. $HCN/NH_3/NO$ was chosen as intermediates resulting from the volatile oxidation reaction, while NO was chosen for char oxidation [37, 38]. The species transport model was used to simulate the continuous phase. The finite rate/eddy dissipation model was used to simulate the combustion reaction of volatiles [6, 19, 25], which calculates both the reaction rate according to the Arrhenius equation and the reaction rate through the turbulent mixing process and uses the smaller of them. Below is the reaction of the combustion mechanism of volatile components and carbon monoxide oxidation by volume reactions

$$C_mH_nO_lN_kS_j + \left(\frac{m-l}{2} + \frac{n}{4} + j\right) O_2 \longrightarrow mCO + \frac{n}{2}H_2O + \frac{k}{2}N_2 + jSO_2 \,,$$

$$CO + 0.5\, O_2 \rightarrow CO_2 \,,$$

where coefficients m, n, l, k, j were received on the basis of coal composition.

Radiation between the boiler walls and the surface of coal particles was taken into account by using the discrete ordinates (DO) model [6, 19, 25,

27]. Emission and radiation heat exchange between coal particles and flue gas were also calculated using the DO model. Radiation transport equations are solved for a finite number of discrete constant angles. Theta and phi division coefficients controlled the accuracy of angular discretization. For theta and phi division coefficients the value of 4 was adopted as well as for theta and phi pixels the value of 3 was set. Radiation calculations were used in each iteration. Table 5 presents the summary of numerical models. Flue gas absorption was taken into account by using the grey gas model [3, 6, 21, 26, 27, 29]. It is estimated based on local concentrations of H_2O and CO_2, thickness of the radiating flue gas layer and total pressure. The calculations assumed a spherical coal shape, and Rosin–Rammler–Sperling distribution was used for its particles [24, 25, 28].

Table 5: Summary of numerical models.

Two-phase model	Euler–Lagrange
Turbulence model	k-ε real
Combustion model of volatile	Finite rate/eddy dissipation
For the coal particle	
Devolatilization	Single-rate model
Combustion of char	Diffusion-kinetic model
Radiation model	DO
NO_x model	
Formation	Thermal and fuel pathways
Concentration of OH and O	Partial equilibrium
PDF turbulence interaction	Temperature mode
Intermediates from volatile	$HCN/NH_3/NO$
Intermediates from char	NO

3 Modelling results

Figure 5 presents a comparison of average flue gas temperatures in cross sections as a function of furnace chamber height.

The average flue gas temperature increases from the slag hopper along the height of the chamber. In the area of coal dust burning, the temperature begins to rise rapidly. The temperature increases for all cases in the area of OFA nozzles – as a result of combustion of unburned fuel particles resulting from substoichiometric combustion. Above the OFA nozzle level, the temperature falls sharply. In the region of the platen superheater at a height of

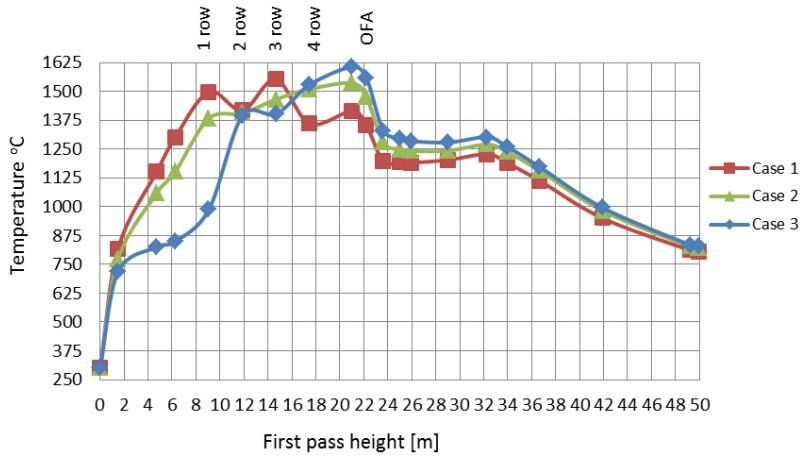

Figure 5: Average flue gas temperature in cross sections of the combustion chamber as a function of its height.

29 m to 32 m flue gas temperature slightly increases. It is caused by mutual heat exchange between water walls and superheater. Then the temperature steadily falls. For case 1, the flue gas temperature reaches the highest value at the third row level of burners – mills M1 and M3 are worked. For case 2, the flue gas temperature reaches the highest value at the OFA nozzle level. Combustion is stretched along the height of the burner belt – mills M1 and M4 worked. For case 3 the flue gas temperature reaches the highest value at OFA nozzles level – mills M2 and M4 worked. For case 1 the average flue gas temperature is higher than for case 2 and 3 in the slag hopper because the burners powered by the mill M1 are worked – see Fig. 5.

Figure 6 shows the flue gas temperature in characteristic planes. Operating boiler with mills M1 and M4 extends combustion along the burner belt to a greater extent than with mills M1 and M3. In option 3, the flame core is shifted up the furnace chamber and the highest temperature at the outlet from the furnace chamber was obtained – Fig. 6 and Table 5.

Figure 7 shows a comparison of the average unit heat flux as a function of the furnace chamber height for the 3 considered cases. For case 1 and 2, the unit heat flow transmitted in the slag hopper is larger than for case 3 because the burners powered by the M1 mill were working.

Figures 8 and 9 present the unit heat flux received by the walls of the first boiler pass. For case 1 (mills M1, M3) the second level of the burners is the most heat loaded. The screen between the fourth row of burners and OFA nozzles on the front wall is the most heat-affected in case 3 (mills M2,

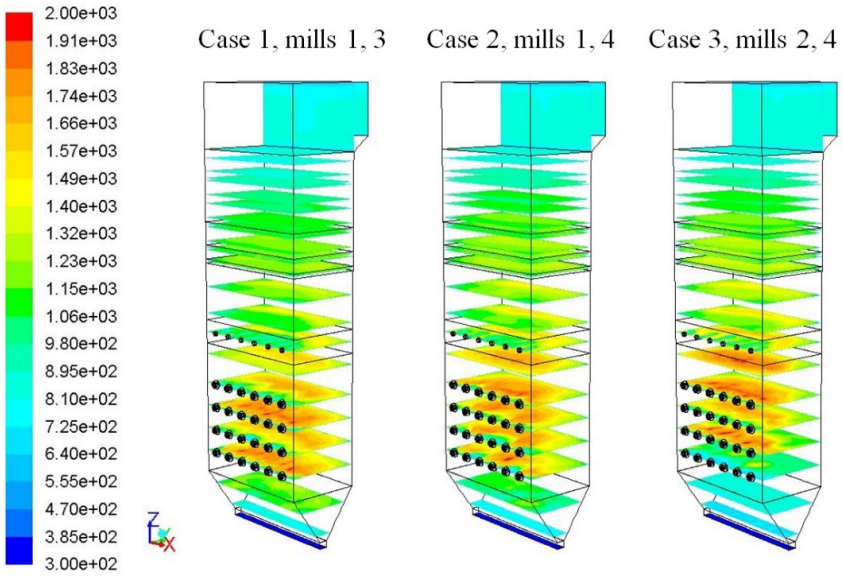

Figure 6: Flue gas temperature in characteristic planes of the first pass of the boiler.

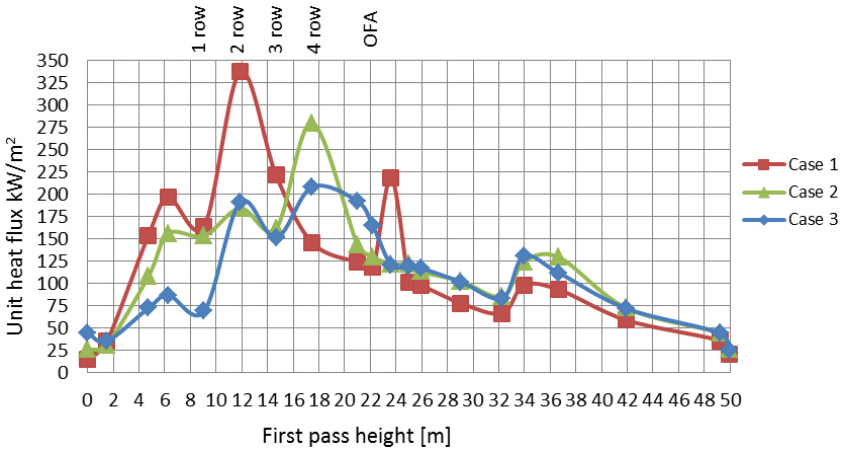

Figure 7: Average unit heat flux in cross-sections of the combustion chamber as a function of its height.

M4). The side walls in case 3 and 2 absorb the most unit heat flux at the second and fourth level of the burners. The slag hopper takes over the least unit heat flux in case 3 because the combustion chamber was powered by mills M2 and M4.

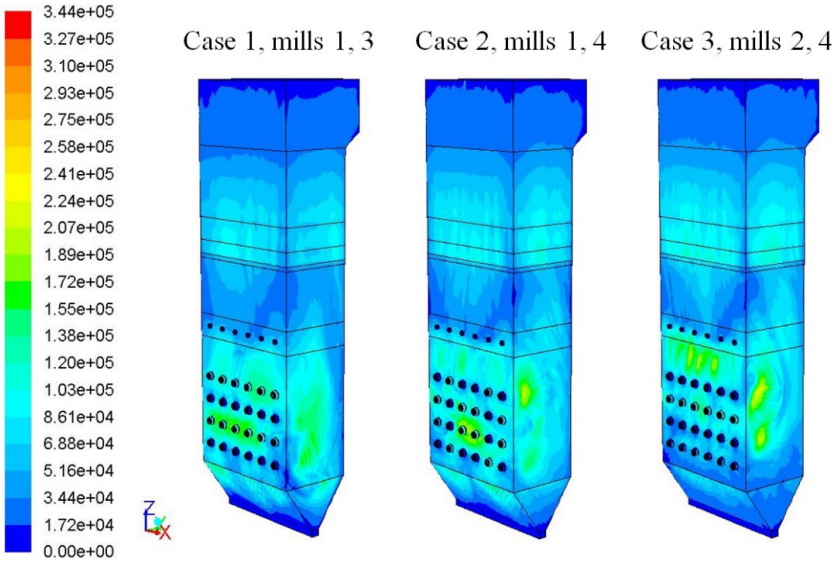

Figure 8: Unit heat flux [W/m^2] received by the front and right walls of boiler.

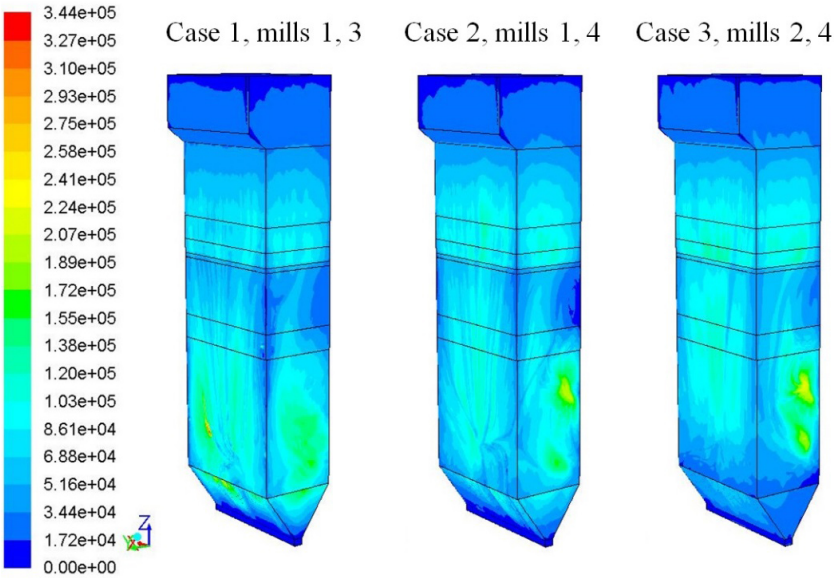

Figure 9: Unit heat flux [W/m^2] received by the rear and left walls of boiler.

Figure 10 presents the O_2 mass fraction in the characteristic planes of the first pass of the boiler. The oxygen content in the combustion chamber

depends on the combustion process. For case 1 on the second and fourth level of burners oxygen coming from the air cooling the inoperative burners was observed. In case 3 operating with mills M2 and M4, oxygen from the inoperative first level of the burners, not taking part in the combustion process with a sufficient degree, accumulated in the slag hopper – Figs. 10 and 11.

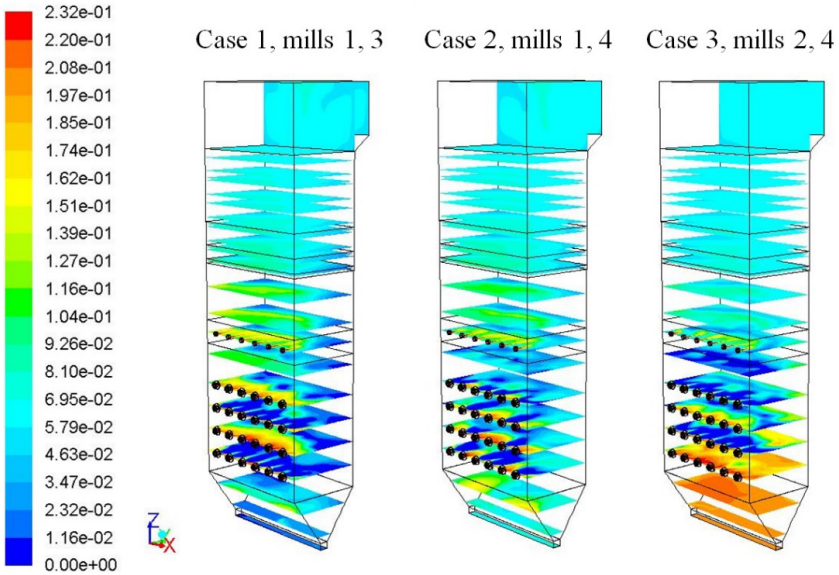

Figure 10: Oxygen (O_2) mass fraction in the characteristic planes of the first pass of the boiler.

Figure 11 presents a comparison of the average oxygen content in the flue gas in cross sections of the combustion chamber as a function of its height.

The decrease in oxygen content for all cases in the region of working burners for particular case is a result of the fuel combustion process. The boiler operation with mills M1 and M3 (case 1) reduces the oxygen content in the flue gas in the slag hopper, and increases from the fourth row of burners compared to case 2 and 3 – see Fig. 11. For all cases, the amount of oxygen in the flue gas increases around the level OFA nozzles. Its reduction occurs there as a result of combustion of unburned fuel particles.

Figure 12 shows the CO content in the characteristic surfaces of the model. Carbon monoxide appears in the area of degassing of coal dust particles in the area of the burner belt of the combustion chamber and in

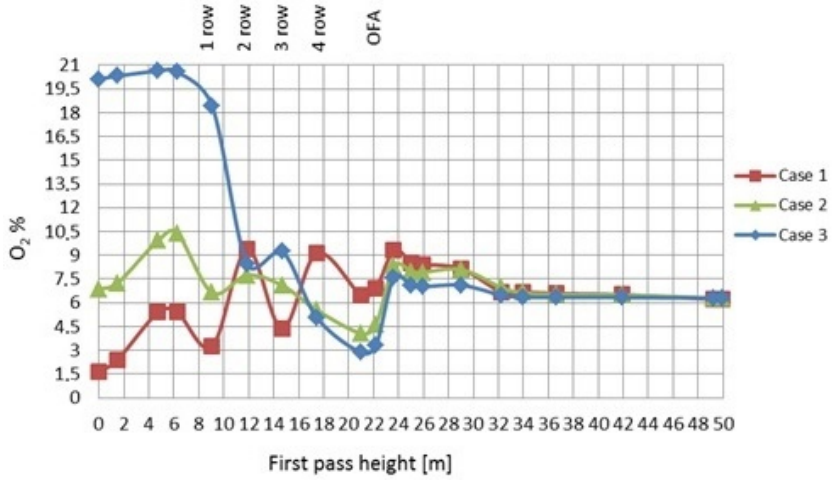

Figure 11: Average oxygen content in flue gas in cross sections of the first pass of the boiler as a function of its height.

the zone of combustion of volatile fraction. The appearance of CO in the area of the burners is also a consequence of combustion of coal dust particles with an oxygen deficiency in the combustion zone – Figs. 12 and 13.

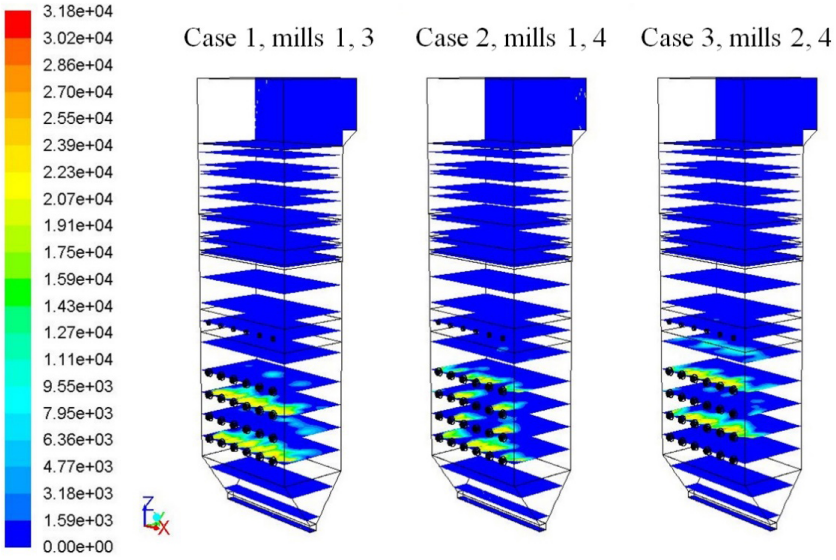

Figure 12: CO fraction in dry flue gas [mg/m^3_n 6% O_2] in the characteristic planes of the first pass of the boiler.

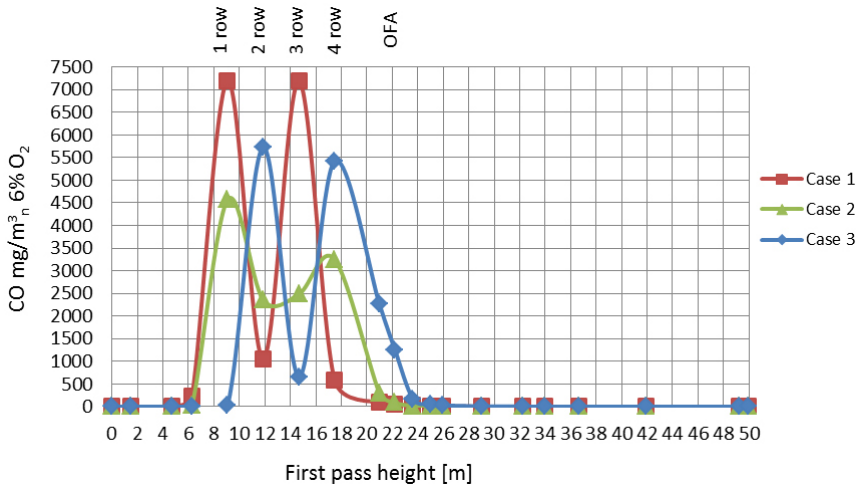

Figure 13: Average content of CO in dry flue gas in cross sections of the first pass of the boiler as a function of its height.

The comparison of the average CO content in dry flue gas in the cross-sections of the first pass of the boiler as a function of its height for the considered cases is presented in Fig. 13. For all cases the mass fraction of CO increases at the level of burners operating in particular cases. This results from the fuel degassing process. The area of inoperative burners but supplied with air cooling as well as the OFA nozzle level are the zone of CO oxidation to CO_2.

Figure 14 presents the share of NO_x in the characteristic surfaces of the first pass of the boiler.

In case 3 (mills M2 and M4) in the slag hopper, the smallest amount of nitrogen oxides is formed – Figs. 14 and 15. This is due to the lower temperature in the hopper for this case – Figs. 5 and 6. A comparison of the average content of nitrogen oxides in dry flue gas in the cross-sections of the first boiler pass as a function of its height for the three considered cases is presented in Fig. 15.

With the flame position rising (from cases 1 to 3) from the 3rd row of burners to the OFA level, the content of nitrogen oxides in dry flue gas increased. After reduction and a slight increase around the platen superheater (because the flue gas temperature increases slightly at this level – Fig. 5), the amount of nitrogen oxides practically does not change – Fig. 15. Despite the lower flue gas temperature for case 2 – Fig. 5 but a higher oxygen

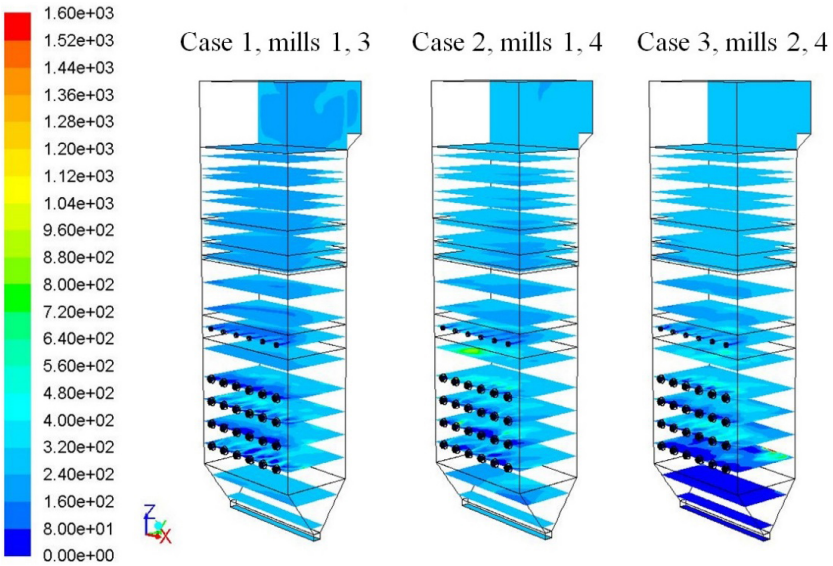

Figure 14: Share of NO_x [mg/m^3_n 6% O_2] in characteristic planes for the first pass of the boiler.

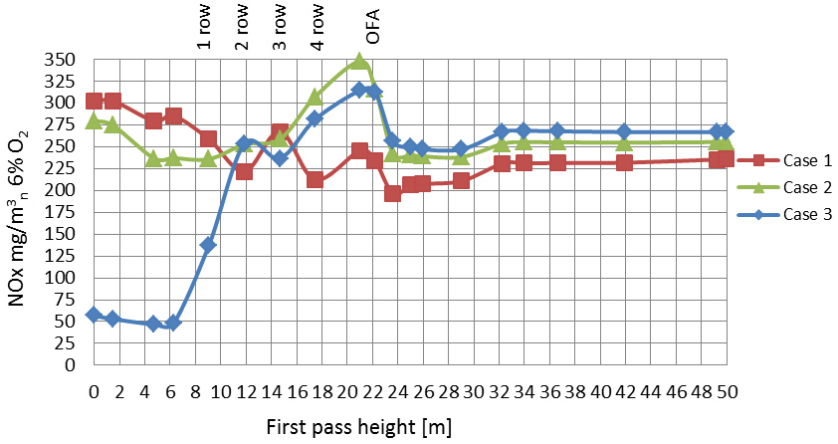

Figure 15: Average NO_x content in dry flue gas in cross sections of the first pass of the boiler as a function of its height.

content – Fig. 11 over the fourth row of burners, the amount of nitrogen oxides in this case in this region is greater than in case 3.

Table 6 summarizes the temperature and amount of O_2, CO, and NO_x in the dry flue gas in the outlet plane of the combustion chamber and in

the outlet plane from the first pass of the boiler. The unburnt carbon (UC) is also showed. Numerically results were obtained at a level close to the calculated and design values of Rafako. Harmful substances such as carbon monoxide and nitrogen oxides were calculated to 6% of O_2 in dry flue gas and presented in mg/m_n^3. Presented values were received as area-weighted average in plane.

Table 6: Comparison of results in the outlet planes of the combustion chamber and first pass of the BP 680 boiler.

Data		Unit	Rafako	Case 1 mills M1, M3	Case 2 mills M1, M4	Case 3 mills M2, M4
				CFD		
O_2 furnace outlet		%	7.1	6.65	6.95	6.47
CO – 6% O_2 model outlet		mg/m_n^3	–	0.94	0.52	3.08
NOx – 6% O_2 model outlet		mg/m_n^3	–	235	255	267
CO – 6% O_2 furnace outlet		mg/m_n^3	–	42	36	48
NOx – 6% O_2 furnace outlet		mg/m_n^3	–	230	253	266
Temperature furnace outlet	mills M1, M3	°C	975	955	997	1028
	mills M1, M4		1003			
	mills M2, M4		1030			
Unburnt carbon	fly ash	%	–	0.8	0.6	0.58
	slag	%	–	2.14	2.46	3.08

Despite the high oxygen concentration in the slag hopper for case 3 but the temperature is too low, according to reaction of char oxidation to CO_2, the fuel did not burn out sufficiently. This results in higher unburnt carbon in slag compared to cases 1 and 2.

As Table 6 showed, boiler operation with a reduced load to 40% affects the increase of oxygen in the flue gas at the combustion chamber outlet in relation to the full boiler load.

For comparison purposes, for 100% full boiler load the individual values for boiler operation on upper (M2, M3, M4) and lower (M1, M2, M3) mills were quoted from [16]. For a 40% load of boiler, oxygen can be seen for individual cases at 6.47 to 6.65%, while for 100% from 2.98% (M2, M3, M4) to 3.5% (M1, M2, M3). Work at low loads also has an impact on the reduction of carbon monoxide emissions in dry flue gas. For a 40% boiler load, carbon monoxide reached values from 48 mg/m_n^3 to 42 mg/m_n^3 and for 100% from 2005 mg/m_n^3 (M2, M3, M4) to 2870 mg/m_n^3 (M1, M2, M3).

Operation of the boiler with 40% load cause a decrease in unburnt carbon in fly ash as well as a slight increase in unburnt carbon in slag compared to work at full load. For a 40% load of boiler, unburnt carbon in fly ash was achieved from 0.58% to 0.8%, while for 100% from 0.76% (M234) to 1.04% (M1, M2, M3). In turn, unburnt carbon in slag for 40% load was achieved from 3.08% to 2.14% and for 100% from 2.86% (M2, M3, M4) to 1.99% (M1, M2, M3). Operation at the technical minimum lowers the average temperature of the flue gas in the furnace chamber to the level of about 1600 °C in comparison to 100% boiler load where the temperature of 1750 °C was occurred. The flue gas temperature at the combustion chamber outlet also decreases for a boiler load of 40% compared to 100%. For 40% load the temperature was obtained from 1028 °C to 955 °C and for 100% load from 1303 °C (M2, M3, M4) to 1273 °C (M1, M2, M3). Similarly, nitrogen oxides decrease with decreasing load. For 40% load they range from 266 mg/m^3_n to 230 mg/m^3_n and for 100% load values from 360 mg/m^3_n (M2, M3, M4) to 298 mg/m^3_n (M1, M2, M3) were obtained.

4 Conclusions

1. Quite good compliance of values obtained from CFD modelling in relation to the values calculated with analytical models in Rafako, in the outlet plane from the combustion chamber of the two-pass ultra-supercritical boiler with front wall swirl burners system – BP 680 boiler – was achieved.

2. Moving the position of the flame core up the furnace chamber (for cases from 1 to 3) increases the temperature, and thus the content of nitrogen oxides in the dry flue gas at the outlet from the furnace chamber and the first pass of the boiler was also increased.

3. Operating of the boiler with mills M1 and M4 (case 2) in relation to mills M1and M3 (case 1) results in an increase in oxygen content and a decrease in carbon monoxide at the outlet from the combustion chamber and the first pass of the boiler.

4. The boiler operation with mills M1 and M3 (case 1) compared to mills M2 and M4 (case 3) results in an increase in oxygen content and a decrease in carbon monoxide at the outlet from the combustion chamber and the first pass of the boiler.

5. Operation of the boiler with mills M1 and M4 (variant 2) compared to mills M2 and M4 (variant 3) results in an increase in oxygen content and a decrease in carbon monoxide at the outlet from the combustion chamber and the first pass of the boiler.

6. The content of the unburnt carbon in fly ash decreases and increases in slag as the flame core moves up the furnace chamber (for cases from 1 to 3).

7. Combustion stability was demonstrated for a minimum boiler load of 40% for three mill system configurations.

8. Based on the numerical research carried out in terms of obtaining the most favourable combustion conditions and the emission of harmful substances, case 1 should be indicated.

Acknowledgments This work is performed within the Applied Research Program – Project: PBS2/B4/8/2013 Low-emission innovative technologies of the upgrade of coal-fired power stations with 200 MW power units.

Received 9 April 2020

References

[1] Directive 2010/75/EU of the European Parliament and of the Council of 24 November 2010 on industrial emissions (integrated pollution prevention and control).

[2] Best Available Techniques Reference Document for the Large Combustion Plants, Final Draft, June 2016.

[3] Sun W., Zhong W., Yu A., Liu L., Qian Y.: *Numerical investigation on the flow, combustion, and NO_x emission characteristics in a 660MWe tangential firing ultra-supercritical boiler*. Adv. Mech. Eng. **8**(2016), 2, 1–13.

[4] Li J., Jankowski R., Kotecki M., Yang W., Szewczyk D., Brzdekiewicz A., Blasiak W.: *CFD Approach for Unburned Carbon Reduction in Pulverized Coal Boilers*. Energy Fuels **26**(2012), 2, 926–937.

[5] Wu X., Fan W., Liu Y., Bian B.: *Optimization of staged combustion in a 600 MWe tangentially fired boiler with wall air injection*. Fuel **275**(2020), 117951.

[6] Tan P., Tian D., Fang Q., Ma L., Zhang C., Chen G., Zhong L., Zhang H.: *Effects of burner tilt angle on the combustion and NO_x emission characteristics of a 700 MWe deep-air-staged tangentially pulverized-coal-fired boiler*. Fuel **196**(2017), 314–324.

[7] Hwang M.-Y., Ahn S.-G., Jang H.-C., Kim G.-B., Jeon C.-H.: *Numerical study of an 870 MW wall-fired boiler using De-NOx burners and an air staging system for low-rank coal*. J. Mech. Sci. Technol. **30**(2016), 12, 5715–5725.

[8] Bar-Ziv E., Saveliev R., Korytnyi E., Perelman M., Chudnovsky B., Talanker A.: *Evaluation of performance of Anglo-Mafube bituminous South African coal in 550 MW opposite-wall and 575 MW tangential-fired utility boilers*. Fuel Process. Technol. **123**(2014), 92–106.

[9] Buchmayr M., Gruber J., Hargassner M., Hochenauer C.: *A computationally inexpensive CFD approach for small-scale biomass burners equipped with enhanced air staging*. Energ. Convers. Manage. **115**(2016), 32–42.

[10] Belošević S., Tomanović I., Crnomarković N., Milićević A., Tucaković D.: *Numerical study of pulverized coal-fired utility boiler over a wide range of operating conditions for in-furnace SO_2/NO_x reduction*. Appl. Therm. Eng. **94**(2016), 657–669.

[11] Żymełka P., Nabagło D., Janda T., Madejski P.: *Online monitoring system of air distribution in pulverized coal-fired boiler based on numerical modeling*. Archives of Thermodynamics **38**(2017), 109–125, DOI: 10.1515/aoter-2017-002.

[12] Chen Z., Wang Q., Wang B., Zeng L., Che M., Zhang X., Li Z.: *Anthracite combustion characteristics and NO_x formation of a 300 MWe down-fired boiler with swirl burners at different loads after the implementation of a new combustion system*. Appl. Energ. **189**(2017), 133–141.

[13] Drosatos P., Nikolopoulos N., Nikolopoulos A., Papapavlou Ch., Grammelis P., Kakaras E.: *Numerical examination of an operationally flexible lignite-fired boiler including its convective section using as supporting fuel pre-dried lignite*. Fuel Process. Technol. **166**(2017), 237–257.

[14] Tsumura T., Okazaki H., Dernjatin P., Savolainen K.: *Reducing the minimum load and NO_x emissions for lignite-fired boiler by applying a stable-flame concept*. Appl. Energ. **74**(2003), 415–424.

[15] Tan P., Fang Q., Zhao S., Yin Ch., Zhang Ch., Zhao H., Chen G.: *Causes and mitigation of gas temperature deviation in tangentially fired tower-type boilers*. Appl. Therm. Eng. **139**(2018), 135–143.

[16] Hernik B., Latacz G., Znamirowski D.: *A numerical study on the combustion process for various configurations of burners in the novel ultra-supercritical BP 680 boiler furnace chamber*. Fuel Process. Technol. **152**(2016), 381–389

[17] Hernik B., Zabłocki W., Żelazko O., Latacz G.: *Numerical research on the impact of changes in the configuration and the location of the over fire air nozzles on the combustion process in the ultra-supercritical BP 680 boiler*. Process Saf. Environ. **125**(2019), 129–142.

[18] Ansys Fluent, Ansys Inc., Canonsburg USA, www.ansys.com.

[19] Choi C.R., Kim C.N.: *Numerical investigation on the flow, combustion and NO_x emission characteristics in a 500 MWe tangentially fired pulverized-coal boiler*. Fuel **88**(2009), 1720–1731.

[20] Drosatos P., Nikolopoulos N., Karampinis E., Strotos G., Grammelis P., Kakaras E.: *Numerical comparative investigation of a flexible lignite-fired boiler using pre-dried lignite or biomass as supporting fuel*. Renew. Energ. **145**(2020), 1831–1848.

[21] Milićević A., Belošević S., Crnomarković N., Tomanović I., Tucaković D.: *Mathematical modelling and optimisation of lignite and wheat straw co-combustion in 350 MWe boiler furnace*. Appl. Energ. **260**(2020), 114206.

[22] Al-Abbas A.H., Naser J., Hussein E.K.: *Numerical simulation of brown coal combustion in a 550 MW tangentially-fired furnace under different operating conditions*. Fuel **107**(2013), 688–698.

[23] Pallare's J., Arauzo I., Williams A.: *Integration of CFD codes and advanced combustion models for quantitative burnout determination*. Fuel **86**(2007), 2283–2290.

[24] He B., Zhu L., Wang J., Liu S., Liu B., Cui Y., Wang L., Wie G.: *Computational fluid dynamics based retrofits to reheater panel overheating of No. 3 boiler of Dagang Power Plant*. Comput. Fluids **36**(2007), 435–444.

[25] Stupar G., Tucaković D., Živanović T., Belošević S.: *Assessing the impact of primary measures for NO_x reduction on the thermal power plant steam boiler*. Appl. Therm. Eng. **78**(2015), 397–409.

[26] Asotani T., Yamashita T., Tominaga H., Uesugi Y., Itaya Y., Mori S.: *Prediction of ignition behaviour in a tangentially fired pulverized coal boiler using CFD*. Fuel **87**(2008), 482–490.

[27] Wang Y., Zhou Y.: *Numerical optimization of the influence of multiple deep air-staged combustion on the NO_x emission in an opposed firing utility boiler using lean coal*. Fuel **269**(2020), 116996.

[28] Wang J., Zheng K., Singh R., Lou H., Hao J., Wang B., Cheng F.: *Numerical simulation and cold experimental research of a low-NO_x combustion technology for pulverized low-volatile coal*. Appl. Therm. Eng. **114**(2017), 498–510.

[29] Yu C., Xiong W., Ma H., Zhou J., Si F., Jiang X., Fang X.: *Numerical investigation of combustion optimization in a tangential firing boiler considering steam tube overheating*. Appl. Therm. Eng. **154**(2019), 87–101.

[30] Zel'dovich Y.B.: *The Oxidation of Nitrogen in Combustion Explosions*. Acta Physicochim URS **21**(1946), 577–628.

[31] Lavoie G.A., Heywood J.B., Keck J.C.: *Experimental and Theoretical Study of Nitric Oxide Formation in Internal Combustion Engines*. Combust. Sci. Tech. **1**(1970), 4, 313–326. DOI: 10.1080/00102206908952211.

[32] Fenimore C.P., Jones G.W.: *The water catalysed oxidation of carbon monoxide by oxygen at high temperatures*. J. Phys. Chem. **61**(1957), 651–654.

[33] Fenimore C.P.: *Formation of Nitric Oxide in Premixed Hydrocarbon Flames*. Symp. (Int.) on Combustion. The Combustion Institute **13**(1971), 1, 373–380.

[34] Westenberg A.A.: *Kinetics of NO and CO in lean, premixed hydrocarbon-air flames*. Comb. Sci. Tech. **4**(1971), 59–64.

[35] Westbrook C., Dryer F.: *Chemical kinetic modelling of hydrocarbon combustion*. Prog. Energy Comb. Sci. **10**(1984), 1–57.

[36] Baulch D.L. *et al.*: *Evaluated kinetic data for combustion modelling*. J. Phys. Chem. Ref. Data **21**(1992), 3, 411–734.

[37] Lockwood F.C., Romo-Millanes C.A.: *Mathematical modelling of fuel – NO emissions from PF burners*. J. Int. Energy **65**(1992), 144–152.

[38] Winter F., Wartha C., Loffler G., Hofbauer H.: *The NO and N_2O formation mechanism during devolatilization and char combustion under fluidized bed conditions*. Symp. Int. on Combustion. The Combustion Institute **26**(1996), 2, 3325–3334.